Tellus (2002), 54A, 426–438
Printed in UK. All rights reserved

Copyright © Blackwell Munksgaard, 2002
TELLUS
ISSN 0280–6495

Generation of equatorial Atlantic warm and cold events in a coupled general circulation model simulation

By W. CABOSNARVAEZ, F. ALVAREZ GARCÍA and M. J. ORTIZBEVIÁ*, *Departamento de Física, Facultad de Ciencias, Universidad de Alcalá, Alcalá de Henares, Madrid 28871, Spain*

(Manuscript received 17 May 2001; in final form 3 December 2001)

ABSTRACT

Warm and cold events in the Gulf of Guinea, characteristic of the tropical interannual variability, can be generated in several ways. This emerges from a statistical analysis of 200 years of interannual variability simulated by a coupled ocean–atmosphere General Circulation Model. The application of a clustering technique to the anomalies of the thermal energy stored in the upper oceanic layers leads to the separation of the events, either warm or cold, into a number of classes, each of them distinguished by a particular generation scheme. The physical mechanisms involved are identified by examining the contributions of the various terms in the mixed layer tendency equation.

Basically, those few classes can be sorted into two larger groups. In one of them, the onset stage is characterized by an eastward propagation of the anomalies. Atmospheric flows play a leading part in the generation of events within this group. In the second group, thermal energy anomalies are generated in situ in the Gulf of Guinea, and it is mixing that gives the most important contribution to the development of the events.

The different classes are related to different seasonal signatures and also to differences in the influence of the El Niño-Southern Oscillation (ENSO). While some of the classes are strongly influenced by ENSO, while in others this influence is not significant. This can explain the barely significant correlations between ENSO and the Atlantic warm events, a feature that the simulation analyzed here shares with the observations.

1. Introduction

The interannual variability of the tropical Atlantic ocean has been shown to be connected to extreme meteorological conditions in Equatorial Africa and North East Brazil, thus strongly impacting on human activities in those areas (Moura and Shukla, 1981; Folland et al., 1986; Wagner and da Silva, 1994).

The most characteristic feature of this variability is the quasi-periodic occurrence of warm events along the equator in the Gulf of Guinea (hereinafter GG), in what looks like an Atlantic analogy of the Pacific El Niño-Southern Oscillation (ENSO). However, this Atlantic mode is not a dominant one, as is the case for ENSO. This makes its study more difficult than that of ENSO. Whether those warmings are actually a manifestation of an ENSO-like coupled atmosphere–ocean mode or a response of the ocean to atmospheric stochastic forcing has been a focus of controversy in recent years.

Using an intermediate coupled model, Zebiak (1993) found that the Tropical Atlantic can support coupled interannual variability that is much similar to ENSO, but has a non-self-sustaining character. Some investigators (e.g. Dommenget and Latif, 2000) point in a different direction, as they explain the Tropical Atlantic interannual

* Corresponding author.
e-mail: mj@ws4.fsc.uah.es

variability in terms of a stochastic driving of the ocean by the atmospheric noise. Support for the thesis of a coupled mode has been provided lately by several works on the observed variability (Chang et al., 2000; Ruiz-Barradas et al., 2000).

Progress in the understanding of ocean–atmosphere interactions has been attained over the last decade due to the great efforts devoted to the study of ENSO in the TOGA program (Anderson et al., 1998). A major achievement rests on the formulation of the delayed oscillator model (Schopf and Suarez, 1988). As the relevance of the role of ocean heat content and subsurface thermal structure became increasingly evident (Chao and Philander, 1993; Latif and Graham, 1992), it served as the conceptual basis for the so-called 'subsurface memory paradigm' (Neelin et al., 1998). Incorporation of new elements is still needed, however, and one single description encompassing all aspects in the variety of behaviour of ENSO in both observations and simulations is as yet unavailable. Such a variety also appears in the events in the Atlantic ocean. As indicated by the forced simulations of Huang et al. (1995), Huang and Shukla (1997) and CabosNarvaez et al. (1998), some of them might follow a scheme parallel to the abovementioned ENSO paradigm: the main features are an accumulation of heat content anomalies in the western equatorial ocean and subsequent eastward propagation later. However, other events in these simulations do not fit into this model. This is also the case for the observed 1963 and 1988 GG warm events in observations of heat content anomalies made available to us by (Carton et al., 2000).

Through the analysis of 200 years of simulated tropical Atlantic variability we aim to elucidate whether a classification of the events into a few different types is possible. The statistical technique we apply, cluster analysis, is basically a classification procedure. As such, it is less constrained towards reduction than other usual techniques, like EOF or POP analysis. Therefore, it seems better suited for the task of capturing the variety of GG events. Finally, evidence for coupled behaviour will be sought by detailed examination of the physics involved in each of the resulting classes.

2. Methodology

Here, we have analyzed a time slice of 200 years, from year 375 to year 575 of a present-day climate simulation with the coupled model ECHAM4-OPYC3. The atmospheric component used for this simulation is the ECHAM4 general circulation model (GCM) developed at the Max Planck Institut für Meteorologie, Hamburg. The oceanic component is OPYC, an isopycnal GCM coupled to a mixed layer and to a sea-ice model (Oberhuber, 1993). Details of this run can be found in Roeckner et al. (1995) or Bacher et al. (1996).

The basic oceanic fields (temperature, salinity, mass vector fluxes, layer thickness for each layer) are saved every 5 days. The contribution of each term in the thermodynamic equation for the mixed layer is saved monthly. Although the vertical resolution is not very high, the model simulates the seasonal cycle quite well. Regarding the interannual timescales with which we are concerned, a quite realistic SST variability is found in the model when compared to observations, as shown in Fig. 1, where we represent the spatial pattern of the two more energetic EOFs of the simulated SST. They explain about 43% of the total variance. These EOFs are similar to the corresponding EOFs of the GISST observations (Dommenget and Latif, 2000), although the observed EOFs explain more variance. In order to identify the occurrence of an event, we require the absolute value of the anomalies to exceed a threshold value of 1.5 times the standard deviation of the GG Index time series for more than 3 months; furthermore, no other previous event should start in the same year (Trenberth, 1997). When this criterium is applied to the observed time series of the tropical Atlantic (GG Index), the warm (cold) events identified agree with those that are accepted in the literature (Servain, 1993). Once the events are spotted from the GG Index, we perform a classification of them based on anomalies of the heat content (hereinafter HC). This is defined as the thermal energy stored in the upper ocean, calculated at each horizontal grid point $\vec{r}_H$ and at each instant of time t as:

$$HC(t, \vec{r}_H) = \rho c_p \int_{h_0}^{0} [T(t, \vec{r}_H, z) - T_0(t, \vec{r}_H)]\, dz \quad (1)$$

where T_0 is the temperature at the h_0 (365 m) depth.

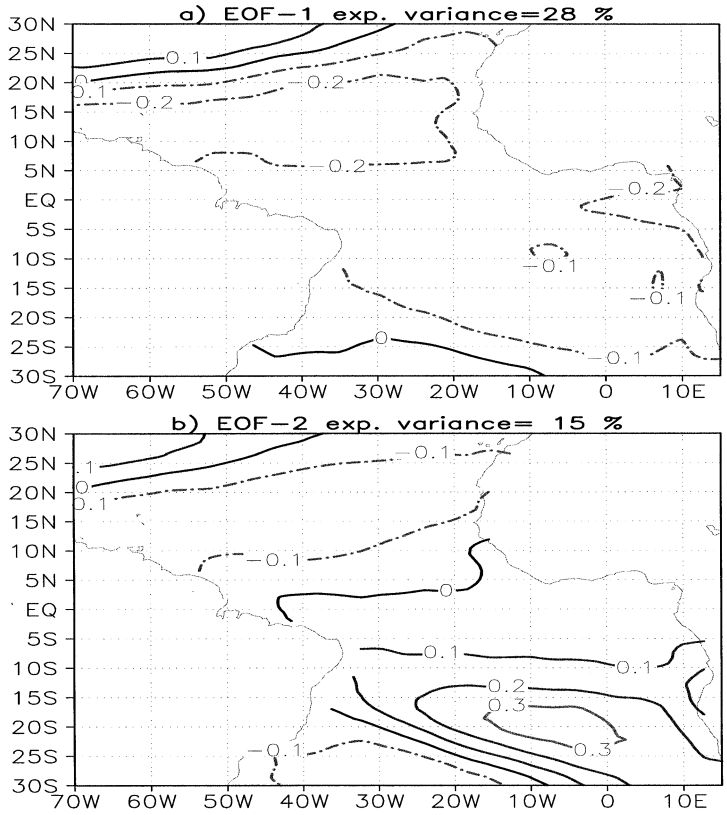

Fig. 1. Upper panel: leading EOF of the 200-year model monthly SST, explaining about 28% of the variance. Lower panel: second most energetic EOF, explaining more than 15% of the total variance.

The HC anomalies have been computed with respect to the 200 year climatology.

The procedure followed is an agglomerative cluster analysis. The criterium for the classification is the minimization of the distance between events, given by:

$$d^l_{gf} = 1 - s^l_{gf}$$

where s^l_{gf} is defined as:

$$s^l_{gf} = \frac{\sum_{j=1}^{N} y_{fj}(t_p - l) y_{gj}(t_p - l)}{\sqrt{\sum_{j=1}^{N} y^2_{fj}(t_p - l)} \sqrt{\sum_{j=1}^{N} y^2_{gj}(t_p - l)}} \qquad (3)$$

Thus defined, the distance d^l_{gf} will vary between 0 and 2.

In the expression above, y_g and y_f stand for the spatial patterns of the HC anomalies in events g and f, respectively, at a certain instant of time. The time t_p is that when the peak of the event under consideration is reached, while l appears as the lag with respect to this peak, which we take as the temporal reference for the analysis of the events. We take for each event $N = 25$ months, begining 16 months before the peak.

At a first stage, when clusters are still undefined, d^l_{gf} has been computed for $l = 3$, 6 and 9 months for every pair of events. The average value of the distance over those three instants has been employed to establish groups initially conformed by a few events with minimum distance (under a threshold of 0.3) among them. Each group is then characterized by a composite built with these first elements, and the usual agglomerating procedure is carried out. The distance to the composites is computed for all the events that remain unclassified, and each one is aggregated to its nearest group. A single lag of $l = 9$ months has been utilized in this second step. Different values of l have been tried in this, as well as in the former

stage, to test the robustness of the classification, with satisfactory results.

The choice of the technique used in this work stems from the recognition that certain patterns are common to the evolution of different events. Although it is known that there is some phase locking to the annual cycle, a detailed analysis of data shows that events can reach their peaks at different seasons. So, characterization of events by means of composites based on calendar months can imply the loss of the information contained in those recurrent patterns. This reasoning led us to the introduction of a timing linked to the peak stage of the events.

Each of these clusters is taken to represent a different class or type of event. To check the classification, and also to try to relate differences among types to the distinct physical mechanisms, we analyze the contributions of the different terms of the thermodynamic equation for the mixed layer (also known as the 'budgets').

From the continuity equation and from the equation describing the temporal evolution of the thermal energy stored in the mixed layer, we can derive another for ρhT, with h being the mixed layer depth (hereinafter MLD), and T and ρ the temperature and density, respectively, within it:

$$\frac{\partial(\rho hT)}{\partial t} = \rho h \nabla \cdot (T\vec{v}) + \vec{\nabla} \cdot [A\vec{\nabla}(\rho Th)] + \frac{Q}{C_p} + [(\omega \rho T)_{up} - (\omega \rho T)_{down}] + Convection \quad (4)$$

where the first term on the r.h.s. represents the advection of temperature due to the oceanic currents. The second stands for the diffusive effect opposite to temperature gradients. The third term introduces the atmospheric heat flux. The fourth represents the interchanges between the mixed layer and the isopycnal layers below, and the last term accounts for convective events, of lesser importance in the tropical Atlantic.

Since heat is distributed throughout the mixed layer column, its depth and density are important elements in determining the way that SST (equivalent in the model to the mixed layer temperature) is affected by heat fluxes. Besides being modified by wind stirring, atmospheric heat fluxes and exchange of heat with lower layers (represented by ω), mixed layer thermal energy is also affected by ocean dynamics.

Furthermore, it is important to realize that when this ω is positive, the mixed layer temperature varies, because the entrained water temperature is different. When ω is negative there is a loss of mass to the underlying layers. Then the (same) atmospheric heat is distributed over a thinner layer and, in absence of any other forcing mechanism, the mixed layer temperature will increase.

3. Results

The scheme used to couple the ocean and atmosphere models ensures that the simulated climatology is close to observations, still allowing the model to show significant decadal and interannual variability (Bacher et al., 1996). The model captures the most important peaks of interannual variability in the GG region, simulating events every 1.5–4 years, with 62 warm events and 53 cold events in our 200-year sample.

A preliminary analysis of the time evolution of the tropical HC shows the existence of similarities among some of the events. In order to isolate events with similar dynamical and thermodynamical properties, we carried out an initial cluster analysis, as stated in our methodology. We found six and five groups of warm and cold events, respectively.

3.1. *Characterization of warm event types*

The result of the cluster analysis in the case of the warm events is summarized in the Table 1, in which we can see that the first and second cluster together account for roughly one half of all the events. The addition of the third, fourth and fifth clusters raises this number to over 80% of all the warm events in the sample. A brief description of the more relevant clusters is given below.

For warm events of the *first cluster*, HC anomalies along the equatorial band, within 5°S and 5°N, 9 months before the event peaks, are positive west of 30°W and negative to the east. In the GG, wind anomalies are eastward at that time. In the next 3 months, a positive HC anomaly builds up west of 20°W, then propagates eastward, reaching the African coast. Strong anomalies then develop and cover the Gulf of Guinea until the event peaks. During the development of these events a positive

Table 1. *Warm event statistics*

Group	N1	D1	V1	N2	D2	V2	ST
I	13	0.36	0.04	49	1.13	0.25	18.5
II	17	0.39	0.05	45	0.95	0.16	33.6
III	6	0.25	0.009	56	1.06	0.24	5.5
IV	4	0.11	0.004	58	0.93	0.26	2.9
V	13	0.40	0.09	49	1.15	0.24	14.3
VI	9	0.70	0.09	53	1.07	0.13	25.2

N1, D1 and V1 denote number of elements, average distance and variance of the latter within a given group, respectively. D1 has been computed using $l = 9$ months in the expression for the distance.

N2, D2 and V2, same as above for events outside a given group. ST, fraction of the total variance explained by a group.

wind-SST feedback can be detected: positive SST anomalies cause the trades to weaken, which in turn enhances the SST anomalies. An analysis of the heat budgets (Fig. 2 later) shows that this comes along with strong positive anomalies of atmospheric heat fluxes and a decrease in the entrainment of cold waters into the mixed layer. Events of this type also present strong HC and wind anomalies north of 10°N. The evolution of HC, SST and zonal wind anomalies at the equator is depicted in the Hoevmoeller diagram of Fig. 3.

For warm events of the *second cluster*, negative HC anomalies cover the equator until 3 months ahead of the peak of the events. Off the equator, at 5°N, east (20°W–10°W), and at 5°S, east (10°W–0°W), positive anomalies are found 10 months before the peak of the event. The latter propagate northward and westward in the following months, whereas the northern anomalies propagate westward, reaching 45°W 6 months before the peak.

In the events belonging to the fifth cluster, at the equator and 10 months before the peak, there are positive HC anomalies to the east, and negative ones to the west. Before the event starts, there is a negative anomaly in the meridional wind, due to the existence of a negative SST gradient. At the same time the MLD decreases. The growth of the event is therefore quite local. In Fig. 4 we have represented the Hoevmoeller diagrams for the evolution of HC anomalies, SST anomalies and zonal wind anomalies at the equator, from 9 months before to 4 months after the peak of the event.

As can be seen in Table 1, the sixth cluster shows a large average distance among its elements. The latter were events which remained unclassified after computations with $l = 9$ months in the procedure described above. Computations with smaller values of l (3, 2 or 1 month; results not shown) revealed that the distance among these residual events reduces drastically at this stage nearer the peak, allowing us to obtain a better defined sixth cluster.

3.2. *Characterization of cold event types*

The result of the cluster analysis in the case of the cold events is summarized by Table 2. There were 10 events of the fourth kind and 16 of the fifth kind, and 9 events in each of the first, second and third kinds in our sample.

A common trait of the warm events was negative MLD anomalies in the GG region 6 or 5 months before the peak. In the case of the cold events, there is not such uniformity: MLD anomalies 6–5 months before the peak were positive only in three out of the five clusters. Events of class first and third show negative MLD anomalies at that time. Nevertheless, such a common trait can be found in another variable: for all the cold events, there were negative SST anomalies at GG at least 5 months before the peak.

In events of the first and second cluster, negative anomalies appear in the west and then propagate to the Gulf of Guinea, where they grow. In events of the third and fourth cluster, the anomalies were generated and grew in the Gulf of Guinea. A brief description of some remarkable features of these types of events follows.

The evolution of HC, SST and zonal wind anomalies at the equator for cold events in the first cluster, prior to and after the peak of the event, is depicted in Fig. 5. Extraequatorial negative HC anomalies converge onto the west of the equator and propagate eastward (12–10 months before the event peaks) and then grow in situ in the Gulf of Guinea. Only this growth is seen in Fig. 5. The most important terms in the Mixed Layer thermal balance are those of mixing and advection. This strong negative mixing term is related to negative MLD anomalies.

Ten months before the start of cold events in the second cluster a positive anomaly propagates from the western equator to the eastern coast.

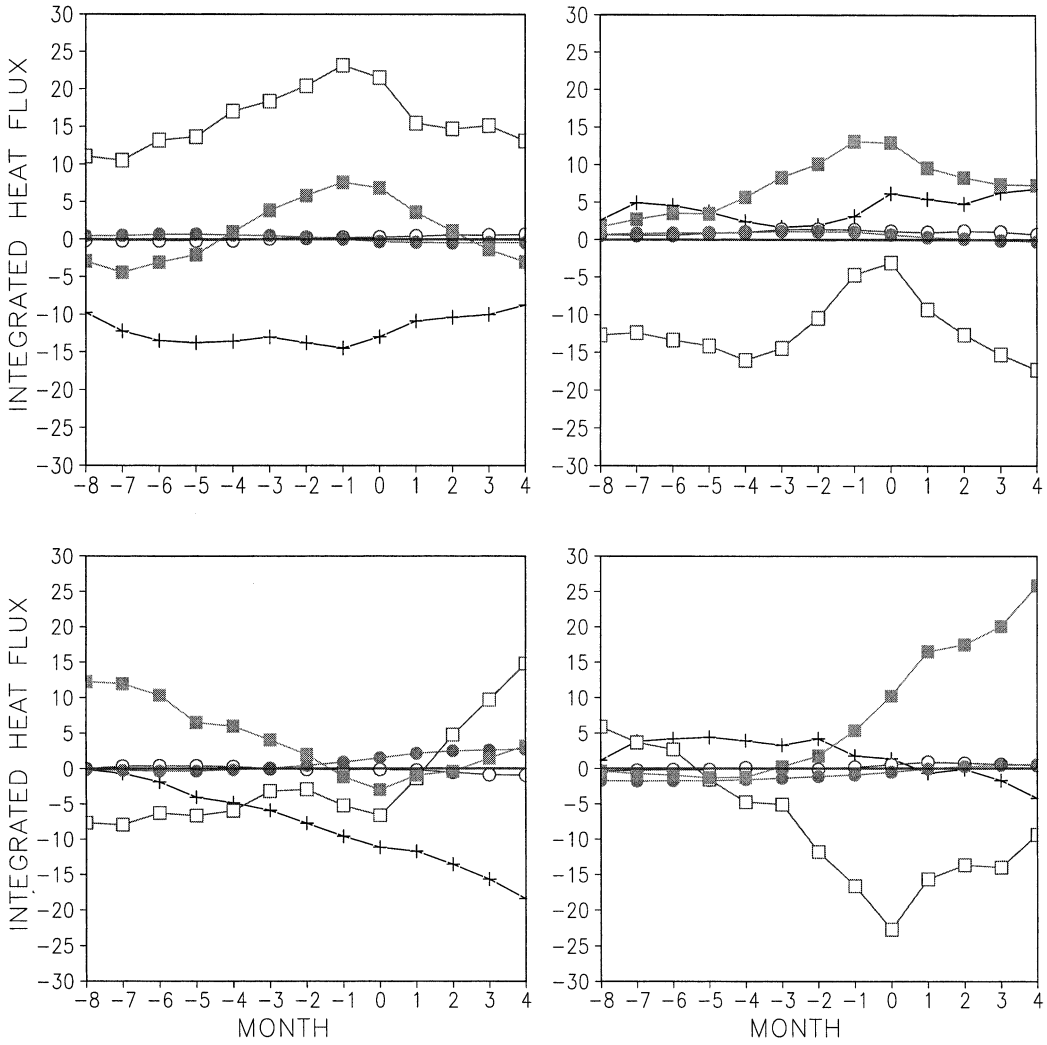

Fig. 2. Accumulated contributions (integrated since 20 months before the peak of the event) of the different terms to the mixed layer heat budget in the Gulf of Guinea. The contributions are spatially averaged over the region [20°W–10°E, 5°S–5°N]: (top left) for the average of warm events in cluster I; (top right) the same for warm events in *cluster 5*; (bottom left) the same for cold events in cluster I; (bottom right) the same for cold events in *cluster 4*. Crosses represent the contribution of advection; full circles, that of diffusion; empty circles, that of convection; empty squares, that of atmospheric heat fluxes; full squares, that of mixing.

From here a cold HC anomaly develops, covering the whole region east of 20°W. The main contribution to the MLD tendency is due to mixing. The atmospheric fluxes have a lesser effect. The strengthening of the zonal and weakening of meridional winds indicate a weakening of the ITCZ.

In the third cluster, events present negative HC anomalies at the equator 10 months before the peak. Two months later, a positive anomaly arises in the west (near the Brazilian coast), simultaneously with the development of a negative anomaly in the east, whose growth and decay originates the event. Wind anomalies are mainly meridional and positive, strengthening the trades. Mixing is giving the most important contribution to the

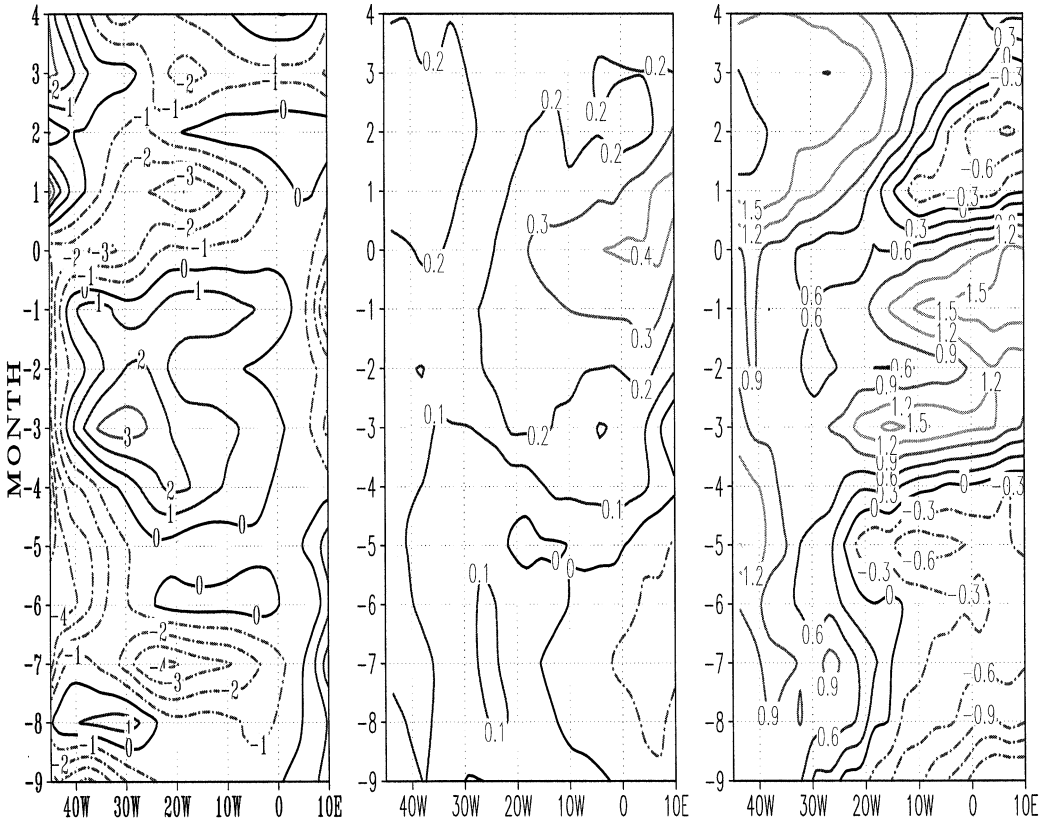

Fig. 3. Hoevmoeller diagram showing the evolution in time of several variables at the equator for the average over the warm events in cluster I. Left: zonal wind anomalies. Center: SST anomalies. Right: heat content anomalies. *X*-axis: longitude. *Y*-axis: months after peak. Notice in the right panel how positive HC anomalies appear in the western equator and then propagate eastward into the GG during months −5 to −3.

MLD tendency. Advection also contributes significantly, while the contribution of the atmospheric fluxes is small.

In cold events in the fourth cluster, 10 months before the peak, HC anomalies are positive all along the equator. Five months before the peak, a positive HC anomaly appears in the west and propagates eastward. The cold SST anomalies present in the event are not in contradiction with these warm HC anomalies, because the MLD anomalies are positive. In Fig. 6, the generation of events of this group is documented through Hoevmoller diagrams for the HC, SST and zonal wind anomalies at the equator. The main contributor to the cooling of the Mixed Layer is the atmospheric heat fluxes, which are negative due to the reinforcement of the zonal winds. The mixing contribution is positive and comparable in magnitude whith atmospheric fluxes. For this type of event, strong mixing tends to heat the Mixed Layer because of the presence of underlying anomalously warm waters, responsible for the positive HC anomalies.

The fifth cluster was built in the same way as the sixth group of warm events, which accounts for the large average distance found in the last row of Table 2. Again high similarity in the stage near the peak was found between events left out of the first four clusters.

3.3. Seasonality and ENSO influence

In observations, most of the warm events peak in summer (defined as June–July–August, JJA),

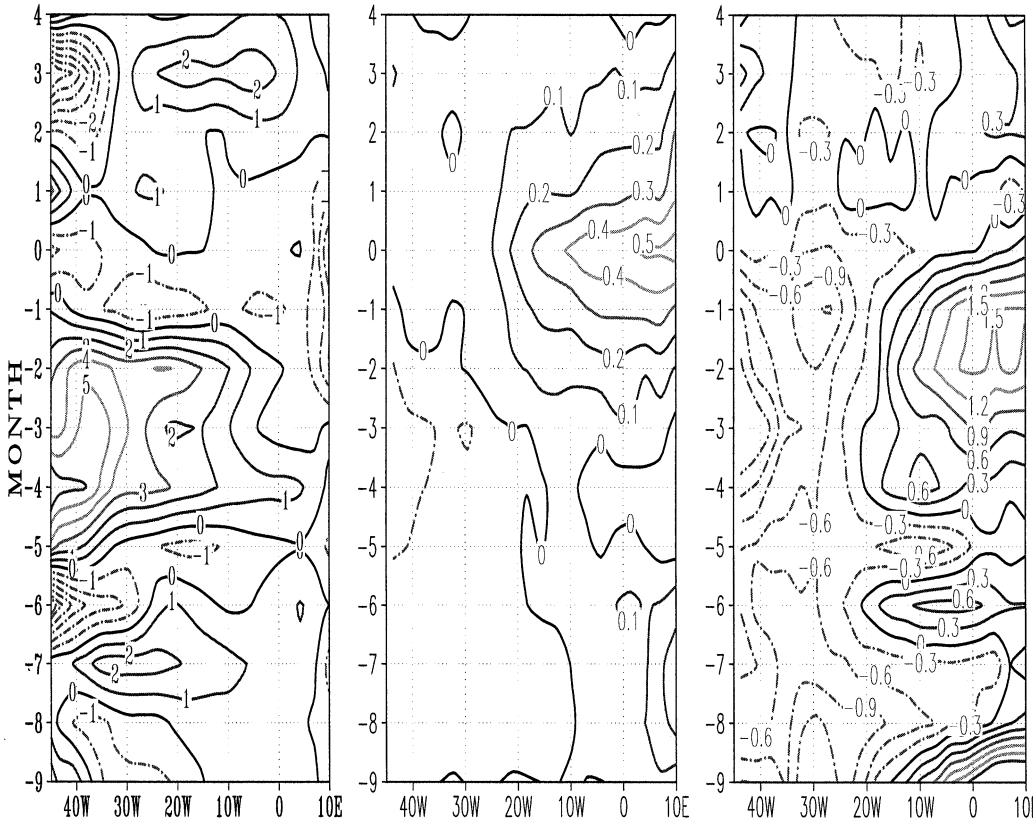

Fig. 4. Hoevmoeller diagram showing the evolution in time of several variables at the equator for the average over the warm events in cluster V. Left: zonal wind anomalies. Center: SST anomalies. Right: heat content anomalies. *X*-axis: longitude. *Y*-axis: months after peak.

Table 2. *Cold event statistics*

Group	N1	D1	V1	N2	D2	V2	ST
I	9	0.47	0.07	44	1.08	0.22	21.7
II	9	0.23	0.03	44	1.12	0.20	9.6
III	9	0.26	0.02	44	1.15	0.20	15.0
IV	10	0.40	0.05	43	1.11	0.21	20.4
V	16	0.77	0.21	37	1.12	0.21	33.2

N1, D1 and V1 denote number of elements, average distance and variance of the latter within a given group, respectively. D1 has been computed using $l = 9$ months in the expression for the distance.

N2, D2 and V2, same as above for events outside a given group. ST, fraction of the total variance explained by a group.

when the thermocline in the GG is shallower. Warm events in the simulation occur one season earlier than in the observations (Table 3). This feature, which also appears in forced simulations (Carton and Huang, 1996; Cabos et al., 1998), can be due to the errors in the modeled seasonal cycle: by spring (March–April–May, MAM), SST in the simulated GG are already warm enough to produce a warm event. Cold events in observations show also a preference to peak in JJA, but some of them take place in MAM. In the simulation cold events also go ahead with respect to the observations and occur in December–January–February (DJF) and MAM.

The impact of ENSO can be assessed through the seasonal correlations at different lags between the Niño3 Index, which monitors ENSO state,

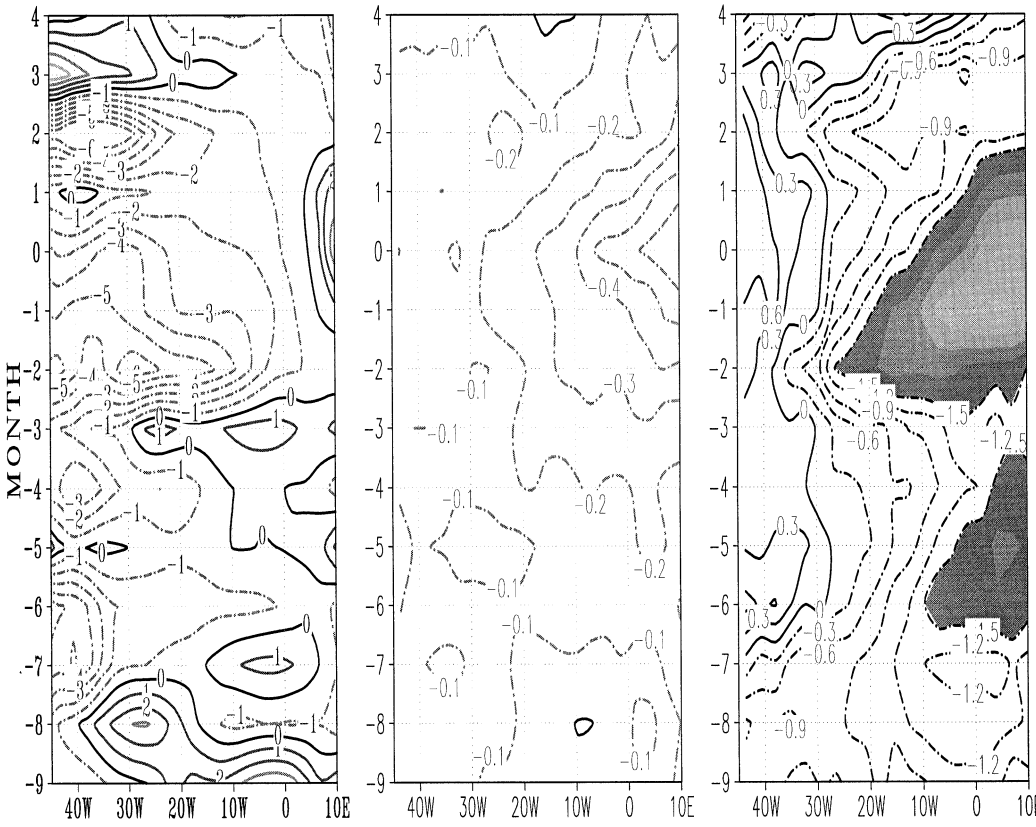

Fig. 5. Hoevmoeller diagram showing the evolution in time of several variables at the equator for the average over the cold events in cluster I. Left: zonal wind anomalies. Center: SST anomalies. Right: heat content anomalies. Values lower than −1.2 are shaded. *X*-axis: longitude. *Y*-axis: months after peak.

and the GG index. The Niño3 Index is built as an average of the SST anomalies within the area (150°W–90°W, 5°S–5°N). To compute these correlations, we have taken into account the values of the Niño3 Index higher than 0.5 K (lower than −0.5 K), i.e. when a warm (cold) event is taking place in the Pacific. The most important features in the observations are the high correlations between the summer (JJA) and autumn (SON) Niño3 anomalies and the winter (DJF) anomalies in the GG, for warm events. These high values of correlations can be explained by a weakening (strengthenging) in the Ekman pumping, induced by changes in the meridional winds. The anticipation in the occurrence of the modeled GG events results in a disagreement between observed and modeled correlations in spring and summer. While for observed cold events a negative correlation occurs between Pacific MAM and Atlantic MAM and JJA, and also between Pacific JJA and Atlantic JJA, this feature is not well captured by the simulation, where negative correlations, found only between MAM and JJA, are too low to be significant.

The different types of events in the simulation also have different seasonality and show a different dependence on ENSO state. In Fig. 7 we have represented the correlations at different lags between SST anomalies of the Niño3 Index and the GG Index, isolating the periods of occurrence of events of distinct types (juxtaposing 19-month-long segments centered at the peak of the events). Warm events of types II, III and IV, which peak mostly in MAM, present significant correlations with the Niño3 Index, the latter leading by 4, 9 and 3 months, respectively. The type I events,

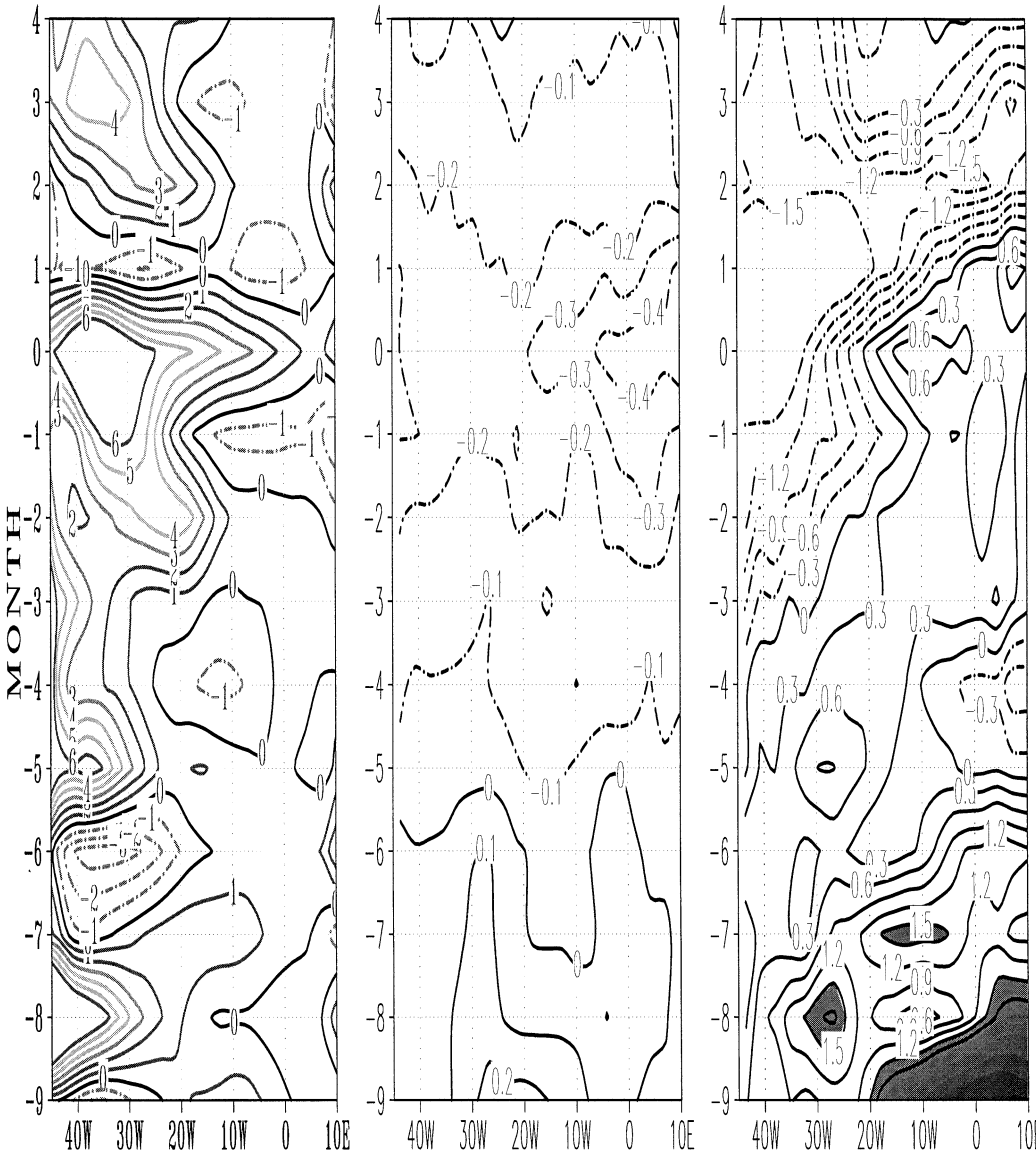

Fig. 6. Hoevmoeller diagram showing the evolution in time of several variables at the equator for the average over the cold events in cluster IV. Left: zonal wind anomalies. Center: SST anomalies. Right: heat content anomalies. Values lower than 1.2 are shaded. *X*-axis: longitude. Y-axis: months after peak. Observe the positive anomalies of HC prior to this type of events.

peaking mostly in DJF, are less significantly correlated with ENSO. As for cold events, those of types II and III present significant correlations with ENSO with highest values at 4 months lag (Niño3 leading).

4. Summary and discussion

The good sampling in both space and time provided by a simulation performed with two coupled GCM (ECHAM4-OPYC3) allows us to

Table 3. *Seasonal distribution of events*

Season	DJF	MAM	JJA	SON
Warm observed	11%	17%	52%	17%
Cold observed	13%	27%	45%	13%
Warm modeled	28%	40%	16%	16%
Cold modeled	25%	35%	23%	7%

The events are sorted by season in which their peak takes place.

identify here a few different ways in which the Gulf of Guinea warmings can be generated. Events (warm or cold) are identified from the Gulf of Guinea Index and the basic variable used for the classification are the tropical HC anomalies. The different kinds of events are identified through a cluster analysis carried on the HC anomalies pattern at nine months before the event peaks.

Each kind of event is characterized through the centroid of its cluster in the HC anomalous field. The evolution in time of this pattern, and the corresponding spatial patterns for the anomalies of other variables, like SST, zonal and meridional winds, give us a dynamical characterization of each type. Likewise, and for each type of event, we obtain the contribution to the mixed layer tendency at different times, before and after the event peaks. These 'budgets', which were saved during the run, not only allow us to further check the differences among event types, but also give us insight into the physical mechanisms at play, responsible for the differences.

Through our statistical analysis, warm events were sorted into six clusters, with four of them explaining roughly 80% of the total number. Cold events were sorted into five clusters, with a comparable weight. Additionally, these clusters can be grouped in two classes, with and without propagating characteristics. Among the warm events, clusters 1, 2, 3 and 6 belong to the propagating class, while 4 and 5 are 'static', non-propagating events. Among the cold events, clusters 1 and 2 belong to the propagating sort, while in all the

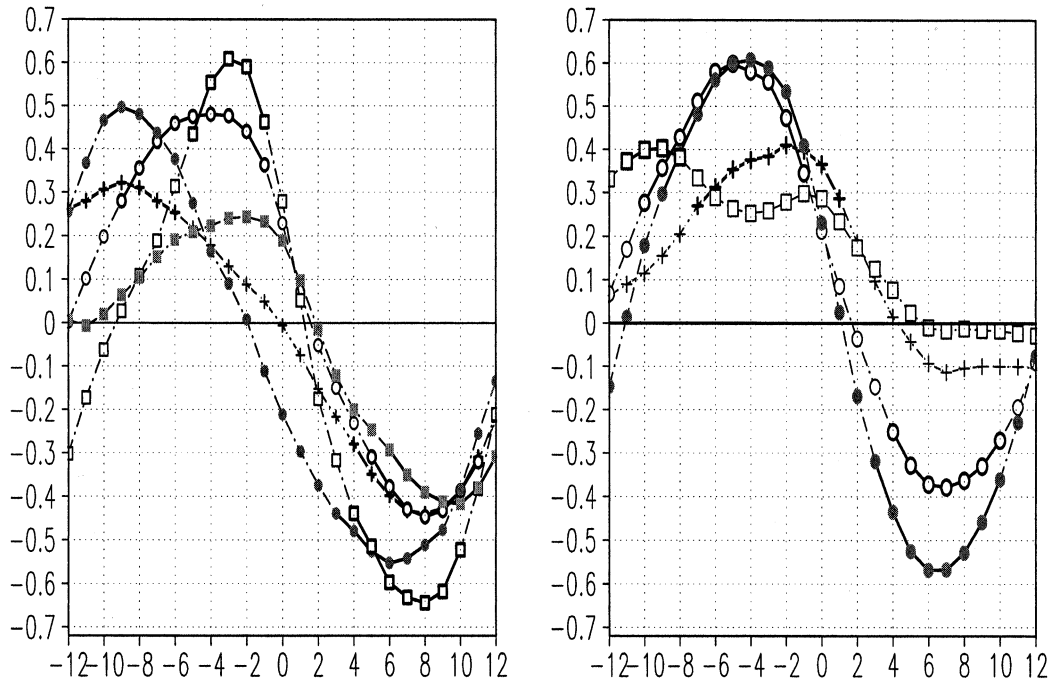

Fig. 7. Correlations between the Niño3 and GG indices for the different types of warm (left panel) and cold (rigth panel). Crosses represent type I events; empty circles, type II; full circles, type III; empty squares, type IV; full squares, type V (for warm events). Solid thick lines correspond to correlation values significantly greater than zero at the 5% confidence level.

others, the HC anomalies are generated and grow in the Gulf of Guinea.

Our analysis detects an important difference with respect to the MLD anomalies between warm and cold events. MLD anomalies before the peak of the event are always negative in the case of warm events. In the case of cold events, MLD anomalies are sometimes positive before the peak: in other cases they are negatives, depending on the class to which the event belongs. Negative mixed layer anomalies contribute to enhancing the effect of atmospheric fluxes. Atmospheric fluxes tend to favour the development of the SST anomalies in the GG in most types of events, in contrast to the damping effect they always play in the evolution of the ENSO anomalies simulated by the present model. This can reflect the fact that local ocean–atmosphere interaction for those events prevails over the effects of the thermocline feedback, although the positive mixing anomalies hint that the latter is still important.

The study of the correlation between the GG and Niño3 indices shows different degrees of influence of Pacific variability for different kind of events. Consistent with their apparently strong connection to atmospheric fluxes (warm SST anomalies contrast with cold HC anomalies), warm events of class IV are highly correlated to ENSO at a short time lag (3 months, Pacific leading). The existence of significant correlations with ENSO at greater lags in the case of events II and III is congruent with the dynamics of those events, where propagating characteristics are important. These differences in the dependence on ENSO explain why the correlation between the GG and Niño3 indices, when computed from the whole sampled length, is not very important. These issues are studied in more detail in a forthcoming paper.

5. Acknowledgments

We thank the DKRZ for the coupled run data. We also thank Dr. J. Oberhuber for the oceanography he taught us in recent years. Thanks are also due to one of the anonymous reviewers for their comments. This work was supported by the European Union Environment and Climate Programme under contract CT98-0714 (SINTEX).

REFERENCES

Anderson, D. L. T., Sarachik, E. S., Webster, P. J. and Rothstein, L. M. 1998. The TOGA decade: reviewing the progress of El Niño research and prediction, *J. Geophys. Res.* **103**, 14,167–14,510.

Bacher, A., Oberhuber, J. M. and Roeckner, E. 1996. ENSO dynamics and seasonal cycle in the tropical Pacific as simulated by the ECHAM4-OPYC3 coupled general circulation model. *Max-Planck-Institut für Meteorologie Report No. 199*, Hamburg.

CabosNarvaez, W. D., OrtizBevia, M. and Oberhuber, J. 1998. The tropical Atlantic variability. *J. Geophys. Res.* **103**, 7475–7489.

Carton, J. A., Chepurin, G. and Cao, X. 2000. A simple ocean data assimilation analysis of the global upper ocean 1950–95. Part II: Results. *J. Phys. Oceanogr.* **30**, 311–326.

Chang, P., Saravanan, R., Ji, L. and Hegerl, G. C. 2000. The effect of local sea surface temperatures on atmospheric circulation over the Tropical Atlantic sector. *J. Climate* **13**, 2195–2216.

Chao, Y. and Philander, S. G. H. 1993. On the structure of the southern oscilation. *J. Climate* **6**, 450–469.

Dommenget, D. and Latif, M. 2000. Interannual to decadal variability in the Tropical Atlantic. *J. Climate* **13**, 777–792.

Folland, C. K., Palmer, T. N. and Parker, D. E. 1986. Sahel rainfall and worldwide sea temperature 1901–1985. *Nature* **320**, 602–607.

Huang, B., Carton, J. A. and Shukla, J. 1995. A numerical simulation of the variability in the tropical Atlantic ocean. *J. Phys. Oceanogr.* **25**, 835–864.

Huang, B. and Shukla, J. 1997. Characteristics of the interannual and decadal variability in a general circulation model of the tropical Atlantic ocean. *J. Phys. Oceanogr.* **27**, 1693–1712.

Latif, M. and Graham, N. E. 1992. How much predictive skill is contained in the thermal structure of an OGCM? *J. Phys. Oceanogr.* **22**, 951–962.

Moura, A. D. and Shukla, J. 1981. On the dynamics of droughts in Northeast Brazil: observations, theory and numerical experiments with a general circulation model. *J. Atmos. Sci.* **38**, 2653–2675.

Neelin, J. D., Battisti, D. S., Hirst, A. C., Jin, F., Wakata, Y., Yamagata, T., Zebiak, S. E. and Anderson, D. 1998. ENSO theory. *J. Geophys. Res. (Oceans)* **103**, 14,261–14,290.

Oberhuber, J. M. 1993. Simulation of the Atlantic circulation with a coupled sea-ice mixed layer – isopycnal general circulation model, I, Model description. *J. Phys. Oceanogr.* **23**, 808–829.

Rayner, N. A., Parker, D. E., Frich, P., Horton, E. B., Folland, C. K. and Alexander, L. V. 2000. SST and sea-ice fields for ERA-40. *Proceedings of the Second WCRP International Conference on Reanalysis*, WCR 109 (WMO/TD-NO.985), 18–220.

Roeckner, E., Oberhuber, J. M., Bacher, A., Cristoph, M. and Kirchner, I. 1995. ENSO variability and atmospheric response in a global coupled ocean–atmosphere GCM. *Max-Planck-Institut für Meteorology Report No. 178*, Hamburg.

Ruiz-Barradas, A., Carton, J. A. and Nigam, S. 2000. Structure of interannual-to-decadal climate variability in the Tropical Atlantic sector. *J. Climate* **13**, 3285–3297.

Servain, J. 1993. Simple climatic indices for the Tropical Atlantic Ocean and some applications. *J. Geophys. Res.* **96**, 15,137–15,146.

Schopf, P. S. and Suarez, M. J. 1988. Vacillations in a coupled ocean–atmosphere model. *J. Atmos. Sci.* **45**, 549–566.

Trenberth, K. E. 1997. The definition of El Niño. *Bull. Am. Meteor. Soc.* **78**, 2771–2777.

Wagner, R. G. and da Silva, A. M. 1994. Surface conditions associated with anomalous rainfall in the Guinea coastal region. *Int. J. Climatol.* **14**, 179–199.

Zebiak, S. E. 1993. Air–sea interactions in the equatorial Atlantic region. *J. Climate* **6**, 1567–1586.